Investigations on structural, magnetic and electronic structure of Gd-doped ZnO nanostructures synthesized using sol–gel technique

Palvinder Kaur[1] · Sanjeev Kumar[2] · Chi Liang Chen[3] · Ying-Ya Hsu[4] ·
Ting-Shan Chan[4] · Chung-Li Dong[4] · C. Srivastava[5] · Anupinder Singh[6] ·
S. M. Rao[1,3]

Abstract $Gd_xZn_{1-x}O$ ($x = 0$, 0.02, 0.04 and 0.06) nanostructures have been synthesized using sol–gel technique and characterized to understand their structural and magnetic properties. X-ray diffraction (XRD) results show that Gd (0, 2, 4 and 6 %)-doped ZnO nanostructures crystallized in the wurtzite structure having space group C_{3v} ($P6_3mc$). Photoluminescence and Raman studies of Gd-doped ZnO powder show the formation of singly ionized oxygen vacancies. X-ray absorption spectroscopy reveals that Gd replaces the Zn atoms in the host lattice and maintains the crystal symmetry with slight lattice distortion. Gd L_3-edge spectra reveal charge transfer between Zn and Gd dopant ions. O K-edge spectra also depict the charge transfer through the oxygen bridge (Gd–O–Zn). Weak magnetic ordering is observed in all Gd-doped ZnO samples.

✉ Sanjeev Kumar
    sanjeev04101977@gmail.com

1   Department of Physics, Punjabi University, Patiala,
    Punjab 147002, India

2   Applied Science Department, PEC University of Technology,
    Chandigarh 160012, India

3   Institute of Physics, Academia Sinica, Taipei 11529, Taiwan

4   National Synchrotron Radiation Research Center (NSRRC),
    Hsinchu 30076, Taiwan

5   Materials Engineering Department, Indian Institute of
    Science, Bangalore 560012, India

6   Department of Physics, Guru Nanak Dev University,
    Amritsar 143005, India

1 Introduction

Zinc oxide (ZnO, wide bandgap ~ 3.37 eV) has transparent properties in the visible range. ZnO is the material having high degree of tunability of charge carriers, carrier mobility, optical transparency and least hazardous to environment (eco-friendly). Consequently, it is widely used in the fabrication of various optoelectronic devices such as transparent conducting oxide (TCO), solar cells or flat panel displays. In order to get better TCO properties of ZnO, it is generally doped with metallic ions (Sn, Ga, In, Al, Sc, etc.) [1–3]. Doping of ZnO with transition metals (TM) such as Fe, Co, N, V and Mn leads to ferromagnetic properties at room temperature (RTFM) [4, 5]. Charge carriers of the semiconductor get spin polarized due to ferromagnetic coupling of the dopant ions [6]. Semiconductors competent of preserving RTFM are potential candidates for industrially feasible spin dependent devices.

Preparation method and conditions strongly affect the ferromagnetic (FM) properties of doped ZnO [7]. Magnetic spins due to dopant ions should be confined to homogeneous sites in the host material. Usually, the origin of the observed FM is still not identified accurately. Some researchers [8–12] reported that the existence of defects like oxygen vacancies must play a key role in the indirect exchange mechanism. RTFM in TM-doped ZnO is strongly interrelated with structural defects and occurs from carrier-mediated exchange coupling [13].

Enhanced ferromagnetism is reported by incorporation of rare earth metals (REMs) such as Gd^{3+} in GaN [14, 15], which inspires the researchers toward REM ion(s) doping in metal oxides for the possible spintronic applications. Reports are available on Gd^{3+}-doped ZnO showing improved room temperature ferromagnetic properties [16–18] due to its 4f state. In addition, these 4f states of Gd are

accountable for enhanced hole conductivity, because the holes in 4f states are more active than electrons [19].

The temperature during preparation, the annealing temperature, the doping concentration and even the matrix grain size are the vital parameters that decide the solubility of a dopant in a matrix [20]. Straumal et al. [21] reported that the cobalt (dopant) solubility in ZnO (matrix) increases with decreasing ZnO grain size. The ionic radius for Gd^{3+} ion (0.094 nm) is bigger than that of Zn^{2+} (0.074 nm). Consequently, inclusion of Gd^{3+} ion in ZnO matrix results in distortion in the ZnO crystal lattice [22–24]. Various reports available with different magnetic behavior in Gd-doped ZnO system motivated us to re-investigate the structural and magnetic behavior of Gd-doped ZnO nanoparticles.

2 Experimental

Gd-doped ZnO nanostructures were synthesized by sol–gel technique. Zinc acetate dihydrate, gadolinium nitrate, 2-methoxyethanol and monoethanolamine (all chemicals were purchased from Sigma Aldrich) were used as the starting materials, solvent and stabilizer, respectively. Zinc acetate dihydrate and gadolinium nitrate were first dissolved in 2-methoxyethanol. The molar ratios of mono-ethanolamine to zinc acetate dihydrate were maintained at 1. Then, the resulting mixture was stirred at 60 °C for 2 h. When the mixture was stirred, monoethanolamine was added drop by drop. Finally, a clear and transparent homogeneous solution was formed. The total concentration of solution was kept at 0.5 mol/L, and the concentration of Gd dopant was 2, 4 and 6 mol% with respect to zinc. The sol was aged for 24 h at room temperature. Then, we dried the sol in a furnace at 500 °C for 1 h and crushed the dry samples in pestle mortar to get the fine powder. Then, we again annealed the fine powder at 500 °C for 1 h to completely remove organic impurities.

The structural properties of Gd-doped ZnO nanostructures were investigated using panalytical X'pert diffractometer. JEOL high-resolution transition electron microscope (HR-TEM) was used for size determination and structural analysis of Gd-doped ZnO nanostructures. Magnetic measurements were taken using a quantum design vibrating sample magnetometer (VSM). The XANES measurements at the Gd L3-edge and Zn K-edge were taken on the BL17C1 and BL01C wiggler beamlines and recorded by the fluorescence yield (FY) at room temperature. Monochromators with Si (111) crystals were used on both the beam lines with an energy resolution $\Delta E/E$ better 2×10^{-4}. The O K-edge absorption spectra were recorded by the total electron yield (TEY) mode at BL20A beamline with $\Delta E/E$–8000 at National Synchrotron Radiation Reach Center (NSRRC) in Taiwan, operated at 1.5 GeV with a current of 200–240 mA. All spectra were normalized to a unity step height in the absorption coefficient from well below to well above the edges. Standard Zn metal foils and oxide powders, ZnO (wurtzite) and Gd_2O_3 were used for energy calibration and also for comparing different electronic valence states.

3 Results and discussion

Figure 1a presents the XRD patterns of sol–gel synthesized Gd-doped ZnO nanostructures. Figure 1b shows the Rietveld refined patterns for Gd-doped ZnO achieved using FullProf software. Pseudo-Voigt function was adopted to carry out Rietveld refinement of all the samples with the space group P63mc. During the Rietveld refinement, wurtzite structure of ZnO was preferred as starting model structure. Table 1 presents the calculated parameters for Gd-doped ZnO nanostructures using Rietveld refinement. XRD patterns show that the Gd doping did not change the crystalline structure of host ZnO. With increase in Gd doping %age, broadening as well as reduction in intensity of diffraction peaks is observed (Fig. 1c). This depicts the weakening of the crystalline structure of ZnO due to increase in Gd doping. Gd oxide usually crystallizes upon annealing the sample at 400 °C, which may be present in very small amount, unable to detect by XRD [7]. Most intense peak corresponding to (101) plane slightly shifted to higher angles with Gd doping. This may be due to the internal compressive stress as reported earlier [7]. They also reported that doping of Gd ions create oxygen vacancies in ZnO host matrix. As a result, lattice parameters will decrease. It is well reported that the presence of oxygen vacancies enhances the presence of RTFM [7].

The average crystallite size is calculated from the full width at half maximum (FWHM) of the intense diffraction peak (101) [calculated using the Scherrer formula; $D = k\lambda/\beta\cos\theta$ where θ is the diffraction angle, β is the FWHM of the diffraction peak, k is the geometric factor (~ 0.9), λ the wavelength of x-ray used and D is the mean crystallite size] is found to be in the range 25–37 nm. Figure 2a shows typical HR-TEM image of Gd-doped ZnO nanostructures. TEM image depicts the nanostructures having different shapes and sizes. It is clearly observed from TEM image that most of the nanostructures are having shape of rods depicting the growth of ZnO wurtzite phase along c-axis. Figure 2b presents the selected area electron diffraction (SAED) pattern confirming the polycrystalline nature of Gd-doped ZnO nanostructures. The varying intensity points observed in the SAED pattern indicate that the Gd-doped ZnO nanostructures consist of crystallites of different size, in corroboration with the crystallite size
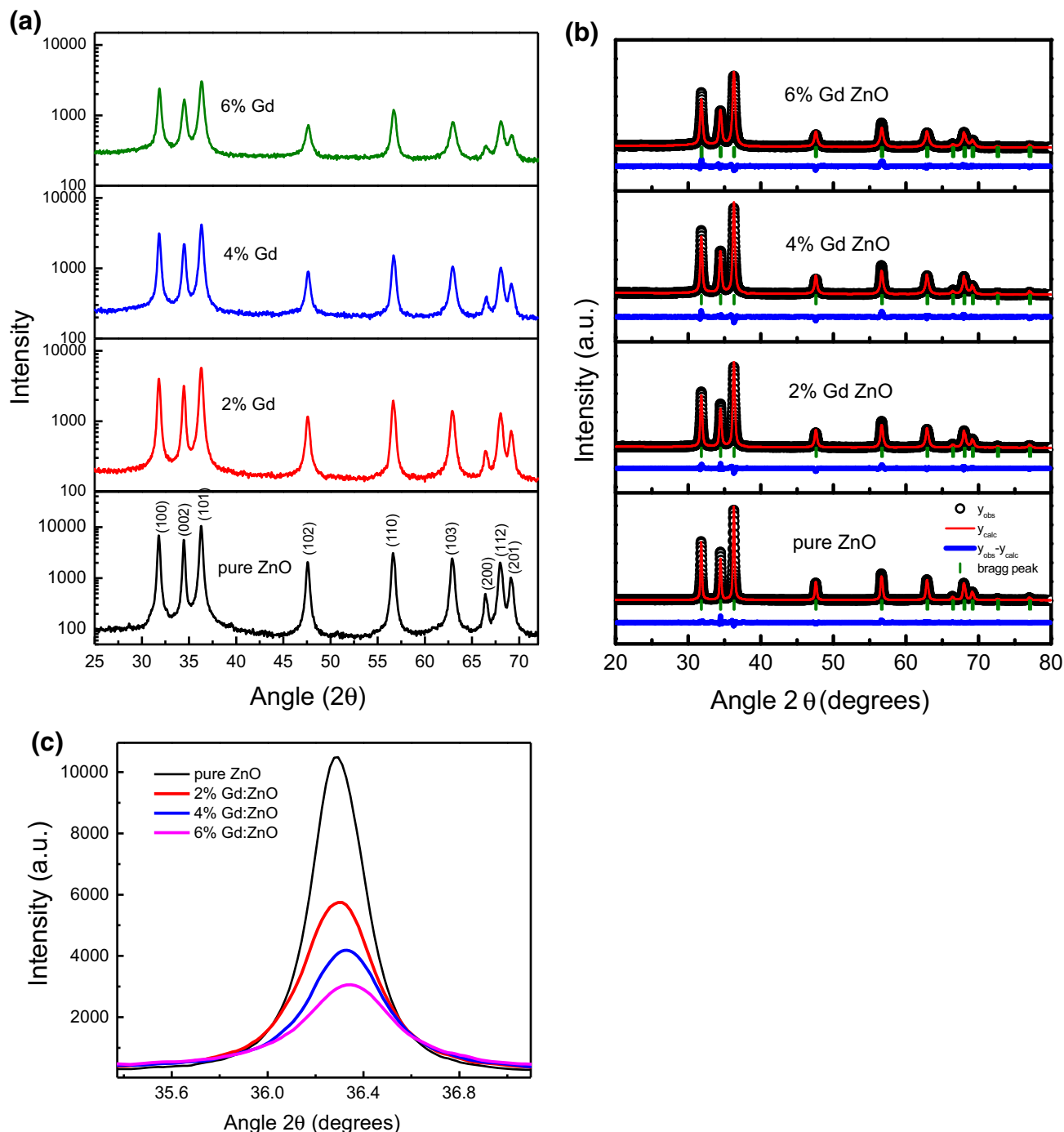
Fig. 1 a XRD patterns for sol–gel synthesized Gd-doped ZnO nanostructures. **b** XRD patterns with Rietveld refinement for Gd-doped ZnO nanostructures. **c** XRD patterns for Gd-doped ZnO nanostructures clearly depicting the peak shift

(25–37 nm) calculated using Scherrer formula and TEM results.

The room temperature photoluminescence (PL) spectra of Gd-doped ZnO nanostructures (Fig. 3a–c) were obtained utilizing a He–Cd laser of 328 nm wavelength as the excitation source. PL spectra are de-convoluted in different peaks responsible for emission. Band edge emission peak is

observed at 384, 387 and 392 nm for 2, 4 and 6 % Gd-doped ZnO samples, respectively. Incorporation of dopant ions introduces a shallow energy level near valence band. The strong violet emission observed around 414 nm in Gd-doped ZnO may be associated with oxygen vacancies [25, 26]. The violet blue emission peak around 452 nm may be credited to the exciton recombination between the holes in

Table 1 Calculated parameters for Gd-doped ZnO nanostructures from Rietveld refinement

Sample	Lattice parameters (Å)			Cell volume (Å^3)	R_p	R_{wp}	R_{exp}	χ^2	Crystallite size D (nm)
	a	b	c						
Pure ZnO	3.249	3.249	5.205	47.595	4.47	5.79	4.22	1.9	36.50
2 % Gd-doped ZnO	3.248	3.248	5.205	47.565	4.65	5.85	5.49	1.14	29.17
4 % Gd-doped ZnO	3.248	3.248	5.206	47.586	4.10	5.46	5.36	1.04	27.78
6 % Gd-doped ZnO	3.248	3.248	5.205	47.574	3.68	5.05	5.22	0.94	25.62
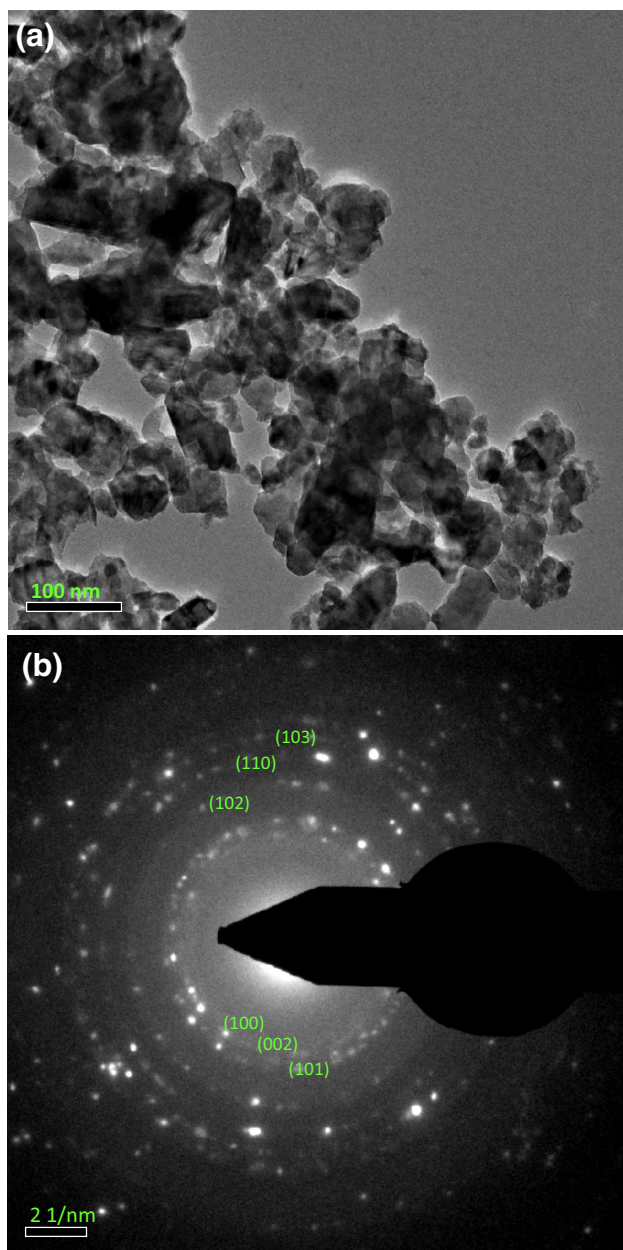
Fig. 2 a TEM micrograph for sol–gel synthesized Gd-doped ZnO nanostructures. **b** SAED pattern for sol–gel synthesized Gd-doped ZnO nanostructures

the valence band and electrons localized at the interstitial zinc [27, 28]. Peak corresponding to 480 nm can be ascribed to intrinsic defects such as interstitial zinc and oxygen [29–31]. Weak green emission peak observed around 520 nm for Gd-doped ZnO may be credited to the transition between singly ionized oxygen vacancy and photoexcited hole, [32, 33] or transition between a deeply trapped hole at V_o^{++} center [34] surface defects [35] and electron close to the conduction band. Green emission is usually related to oxygen deficiency while yellow/orange emission is related to excess oxygen [36].

According to the group theory, wurtzite ZnO belongs to the space group C_{6v} with two formula units per primitive cell. A primitive ZnO cell has four atoms (two formula units), each of which occupies C_{3v} sites, leading to 12 phonon branches (nine optical and three acoustic) [37]. Figure 4 presents the Raman spectra for Gd-doped ZnO nanostructures. Raman active modes at 448 cm^{-1} for E_2 (high), 573 cm^{-1} for 1st order A_1 (LO), 747 cm^{-1} for A_1 (LA + TO) are observed for sol–gel synthesized Gd-doped ZnO nanostructures. The broad peak at about 446 cm^{-1} is reported to the high-frequency branch of the E_2 mode, i.e., E_2 (high) of ZnO, which is a Raman active mode in the wurtzite crystal structure. Stress induced due to Gd doping in the ZnO wurtzite structure affects the E_2 phonon frequency [38]. An increase in the E_2 phonon frequency is ascribed to compressive stress, whereas a decrease in the E_2 phonon frequency is ascribed to a tensile stress. We also observed that increase in E_2 phonon frequency attributes to compressive stress. It is clearly depicted from the observed Raman spectra that there are broadening and shifting in Raman peaks with Gd doping. Chetri et al. [39] reported similar behavior based on Heisenberg uncertainty principle. They reported the relationship between phonon position and crystallite size as $\Delta x \, \Delta p \geq h/4\pi$, where Δx is the crystallite size and Δp is the phonon momentum distribution. The confinement of the phonon within the particle increases, with decrease in the particle size, and hence, the phonon momentum distribution increases with decrease in crystallite size. This phonon dispersion results in asymmetric broadening and shifting of Raman peaks toward lower wavenumber [40].
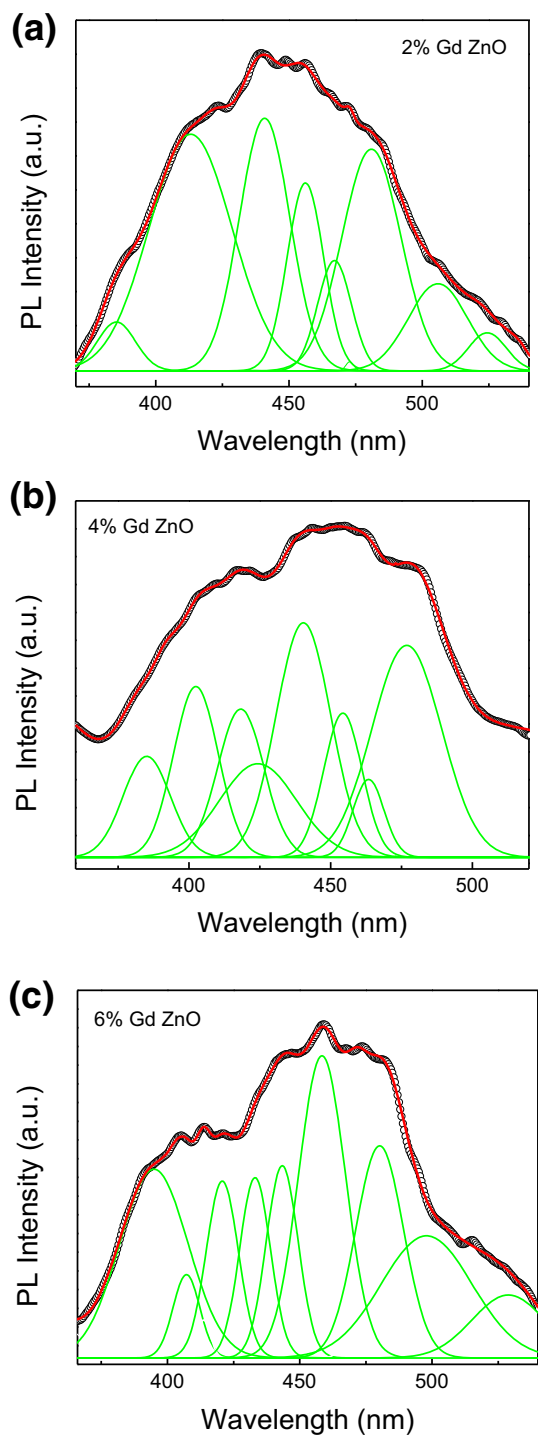
(a) 2% Gd ZnO

(b) 4% Gd ZnO

(c) 6% Gd ZnO

Fig. 3 **a–c** Room temperature photoluminescence (PL) spectra for Gd-doped ZnO nanostructures

Fig. 4 Room temperature Raman spectra for sol–gel synthesized Gd-doped ZnO nanostructures

Figure 5a shows the near-edge features of the Zn K-edge spectra of ZnO with different Gd content 2, 4, 6 % and ZnO standards. The main peak in the photon energy of 9655–9675 eV region is the electronic transition from Zn 1s to the Zn 4sp states. The spectra show the similar line shape and do not observe a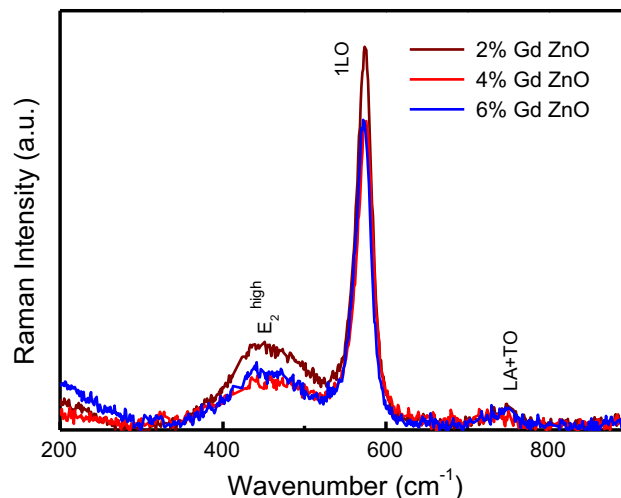ny chemical shift, which depicts that the host ZnO maintained the wurtzite phase with Zn^{2+}. However, since the area under the absorption feature represents the unoccupied states, the evolution of intensity of the main peak shows the change in the hole concentration. The inset of Fig. 5a shows the magnified view of the main absorption peak 'A.' The increase in intensity peak 'A' at 9668.6 eV reveals the enhancement in the Zn 4p unoccupied states as a function of Gd doping. Notably, the number of 4p holes is closely correlated with the carrier concentration. Therefore, the Zn 4p unoccupied states are crucial for the electron transport (or conduction). Further, XANES Zn K-edge spectra are sensitive to the valence state and local environment of Zn ions.

The Gd L_3-edge (transition from $2p_{3/2}$ to 5d) XANES spectra (Fig. 5b) is mostly related to the partial density of 5d unoccupied states. Compared with the standard of Gd_2O_3 (Gd^{3+}), the spectra of doped nanostructures have shown the lower energy shifting. It implies that the Gd may possess the $2 + (4f^7 5d^1)$ with a spin 1/2 electron as inserted in the ZnO. The evolution of the peak 'B,' the inset of Fig. 5b, provides a reasonable estimate of the hole concentration. The total unoccupied states (peak 'B' intensity) decrease in the order 2, 4 and 6 %, which is opposite to the trend observed in Zn K-edge spectra. The decrease in the intensity of peak 'B' and the increase in intensity of peak 'A' increase in Zn K-edge results due to the local inhomogeneity which is further resulting in electron hopping in the orbital of Zn 4p and Gd 5d states. Therefore, the variation in the number of 5d electrons is closely related to the magnetic behavior. The critical and corresponding intensity change in the Zn K-edge and Gd L_3-edge features upon Gd ions substitution is consequently indicative of an increase in the 4p holes and a decrease in
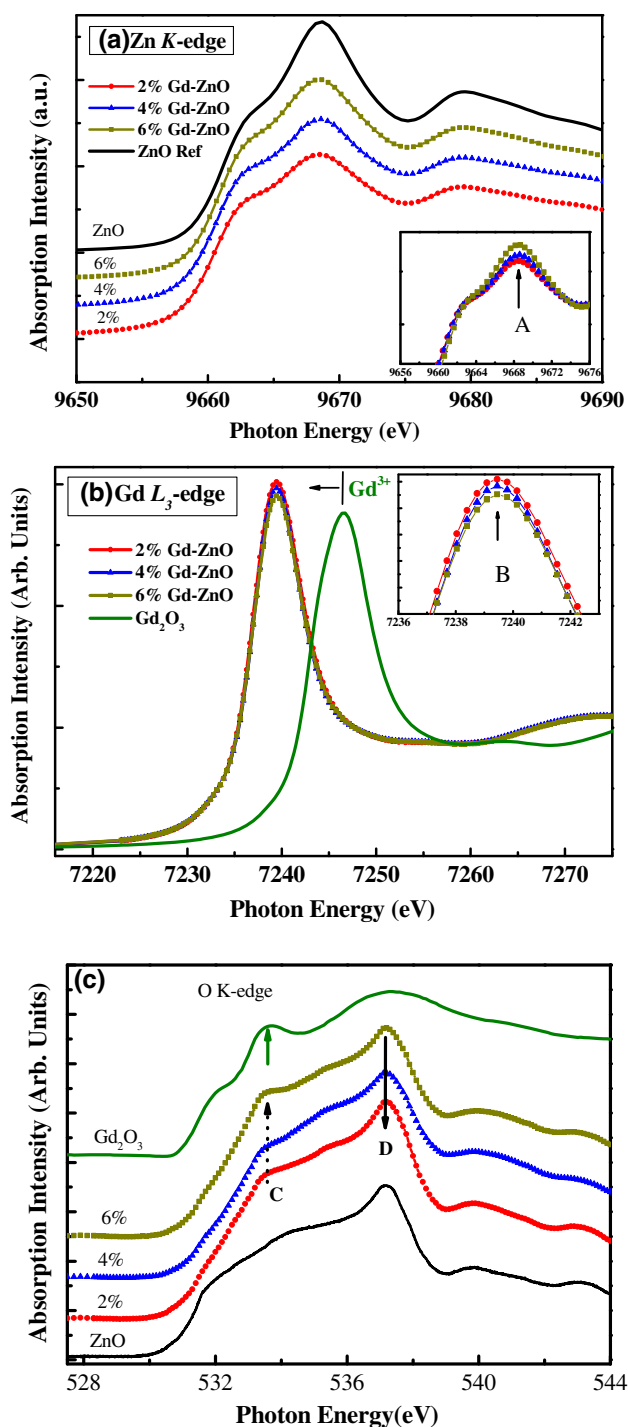
Fig. 5 **a** Zn K-edge spectra for Gd-doped ZnO nanostructures. **b** Gd L edge spectra for Gd-doped ZnO nanostructures. **c** O K-edge spectra for Gd-doped ZnO nanostructures

the 5*d* holes. These spectral changes may arise from charge transfer between host Zn and Gd dopant ions.

O K-edge XAS spectra of pure and Gd-doped ZnO nanostructures are shown in Fig. 5c. The peaks in the energy range between 530 and 540 eV are attributed to the

hybridization of O 2*p*–Zn 4*sp* and Gd 5*d* states. It is observed that the intensities of all the dopant spectra are different from ZnO. The feature 'C' is revealed as the pre-peak of Gd_2O_3 (marked as arrow in the figure), which has full empty *d* orbital. However, the photon energy of peak 'C' is shifted to lower energy site. The shift of peak 'C' suggested a strong hybridization of O 2*p* orbitals with Gd 5*d* states which further indicates that the Gd valence state is different from the Gd_2O_3 as observed in Gd L_3-edge. The intensity of the peak 'C' is increased and that of peak 'D' (transition from O 1 s to the hybridization of O 2*p* and Zn 4*p* state) is decreased. A systematical evolution of these spectral features with Gd doping suggested the presence of electron hopping. The Gd in ZnO matrix induces a strong hybridization of s–p–d orbitals. The charge transfer may take place through the oxygen bridge (Gd–O–Zn), and therefore, the presence of holes should exist at oxygen site.

Figure 6 presents M–H curves for Gd-doped ZnO nanostructures at room temperature. Inset of the figure clearly depicts weak ferromagnetic ordering for all samples. Pure ZnO is showing the mixture of weak ferromagnetic and diamagnetic behavior. The observed diamagnetic behavior increases with increase in applied field. Gd-doped ZnO nanostructures exhibit the mixture of weak ferromagnetic and paramagnetic behavior as observed [41]. With increase in Gd doping beyond 4 %, anti-ferromagnetic behavior comes into the picture. As seen from XRD results, increase in Gd doping deteriorates the crystalline structure of host ZnO. Gd enters into some interstitial positions in host ZnO matrix, resulting in decrease in Gd–Gd distance, which further results in anti-ferromagnetic behavior with decrease in remnant value.

As reported earlier [7], room temperature magnetization in case of Gd-doped ZnO nanoparticles synthesized using
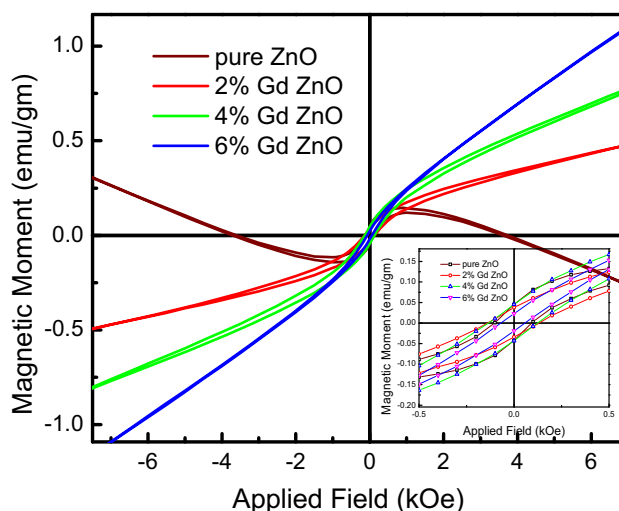

Fig. 6 M–H curves for sol–gel synthesized Gd-doped ZnO nanostructures at room temperature

thermal decomposition method originates from coupled (ferromagnetic) and uncoupled (paramagnetic) Gd dopant ions. Similar behavior is observed in sol–gel synthesized Gd-doped ZnO nanostructures. Kumar et al. 2014 [42] reported the synthesis of Gd-doped ZnO nanoparticles using chemical co-precipitation technique. They observed systematic increase in magnetization with increase in Gd doping %age. Venkatesh et al. [43] also reported that oxygen deficiency-related defect complexes to be responsible for ferromagnetic exchange. Bantounas et al. [44, 45] used density functional theory within the generalized gradient approximation to study the spatial arrangement and magnetic ordering of Gd impurities in a wurtzite ZnO host. Their magnetic results showed mainly paramagnetic (PM) behavior for Gd-doped ZnO and the weak exchange coupling. The observed weak magnetic ordering in Gd-doped ZnO nanostructures is mainly due to the Gd ions substitution for Zn in the ZnO host lattice and not due to Gd metal cluster-like phases as confirmed by the XRD and XAS studies. An exchange mechanism may be associated with defects such as oxygen and zinc vacancies, which is responsible for the weak ferromagnetic ordering in the $Zn_{1-x}Gd_xO$ as depicted by the PL studies in the present work. O K-edge of XAS data has a pre-edge feature at 533.2 eV in all of the samples which is attributed to the oxygen vacancies [46].

4 Conclusions

Nanostructures of $Gd_xZn_{1-x}O$ ($x = 0$, 0.02, 0.04 and 0.06) have been synthesized using sol–gel technique. XRD patterns depicts that the Gd-doped ZnO nanostructures crystallized in the wurtzite structure without formation of any secondary phase. PL and Raman studies of Gd-doped ZnO nanostructures confirm the presence of singly ionized oxygen vacancies which may account for the observed weak magnetic ordering in 2 % Gd-doped ZnO. X-ray absorption spectroscopy (XAS) reveals that Gd replaces the Zn atoms in the host lattice and maintains the crystal symmetry with slight lattice distortion. Gd-doped ZnO samples show paramagnetic behavior with weak ferromagnetic component for low Gd doping, which further converted to anti-ferromagnetic behavior with weak ferromagnetic component for high Gd doping.

References

1. P.K. Sharma, R.K. Dutta, A.C. Pandey, S. Layek, H.C. Verma, Effect of iron doping concentration on magnetic properties of ZnO nanoparticles. J. Magn. Magn. Mater. **321**(17), 2587–2591 (2009)

2. J.H. Shim, T. Hwang, S. Lee, J.H. Park, S.J. Han, Y.H. Jeong, Origin of Ferromagnetism in Fe- and Cu-Codoped ZnO. Appl. Phys. Lett. 86(8), 082503/1–3 (2005)

3. S.J. Yang, A.B. Pakhomov, S.T. Hung, C.Y. Wong, Room temperature magnetism in sputtered (Zn, Co)O films. IEEE Trans. Magn. **38**, 2877 (2002)

4. S.J. Pearton, D.P. Norton, M.P. Ivill, A.F. Hebard, J.M. Zavada, W.M. Chen, I.A. Buyanova, Ferromagnetism in transition metal doped ZnO. J. Electron. Mater. **36**(4), 462–471 (2007)

5. K. Ip, R.M. Frazier, Y.M. Heo, D.P. Norton, C.R. Abernathy, S.J. Pearton, Ferromagnetism in Mn- and Co- implanted ZnO nanorods. J. Vac. Sci. Technol. B **21**, 1476–1481 (2003)

6. K. Potzger, S. Zhou, F. Eichhorn, M. Helm, W. Skorupa, A. Mucklich, J. Fassbender, Ferromagnetic Gd-implanted ZnO single crystals. J. Appl. Phys. 99(6), 063906/1–5 (2006)

7. A.A. Dakhel, M. El-Hilo, Ferromagnetic nanocrystalline Gd-doped ZnO powder synthesized by coprecipitation. J. Appl. Phys. 107(12), 123905/1-6 (2006)

8. M. Venkatesan, C.B. Fitzgerald, J.G. Lunney, J.M.D. Coey, Anisotropic ferromagnetism in substituted zinc oxide. Phys. Rev. Lett. **93**, 177206–177209 (2006)

9. M. El-Hilo, A.A. Dakhel, A.Y. Ali-Mohamed, Room temperature ferromagnetism in nanocrystalline Ni-doped ZnO synthesized by co-precipitation. J. Magn. Magn. Mater. **321**, 2279–2283 (2009)

10. S. Zhou, K. Potzger, A. Mucklich, F. Eichhorn, M. Helm, W. Skorupa, J. Fassbender, Structural and magnetic properties of Tb implanted ZnO single crystals. Nucl. Instrum. Methods Phys. Res. B **266**, 589–593 (2008)

11. J. Qi, Y. Yang, L. Zhang, J. Chi, D. Gao, D. Xue, Room-temperature ferromagnetism in Er-droped ZnO thin films. Scr. Mater. **60**, 289–292 (2008)

12. B.B. Straumal, A.A. Mazilkin, S.G. Protasova, A.A. Myatiev, P.B. Straumal, G. Schütz, P.A. van Aken, E. Goering, B. Baretzky, Magnetization study of nanograined pure and Mn-doped ZnO films: formation of a ferromagnetic grain-boundary foam. Phys. Rev. B **79**, 205206 (2009)

13. F. Pan, C. Song, X.J. Liu, Y.C. Yang, F. Zeng, Ferromagnetism and possible application in spintronics of transition-metal-doped ZnO films. Mater. Sci. Eng. R **62**, 1–35 (2008)

14. S. Dhar, O. Brandt, M. Ramsteiner, V.F. Sapega, K.H. Ploog, Colossal magnetic moment of Gd in GaN. Phys. Rev. Lett. 94, 037205/1–4 (2005)

15. S. Dhar, L. Perez, O. Brandt, A. Trampert, A.H. Ploog, J. Keller, B. Beschoten, Gd-doped GaN: a very dilute ferromagnetic semiconductor with a Curie temperature above 300 K. Phys. Rev. B **72**, 245203/1–9 (2005)

16. A. Garcia-Murillo, C.L. Luyer, C. Dujardin, T. Martin, C. Garapon, C. Pedrini, J. Mugnier, Elaboration and scintillation properties of Eu^{3+}-doped Gd_2O_3 and Lu_2O_3 sol-gel films. Nucl. Instrum. Methods A **486**, 181–185 (2002)

17. A. Garcia-Murillo, C.L. Luyer, C. Garapon, C. Dujardin, E. Bernstein, C. Pedrini, J. Mugnier, Optical properties of europium-doped Gd_2O_3 waveguiding thin films prepared by the sol-gel method. Opt. Mater. **19**, 161–168 (2002)

18. K. Potzger, S. Zhou, F. Eichhorn, M. Helm, W. Skorupa, A. Mcklich, J. Jassbender, T. Herrmannsdorfer, A. Bianchi, Ferromagnetic Gd-implanted ZnO single crystals. Appl. Phys. Lett. 99, 063906/1–5 (2006)

19. L. Liu, P.Y. Yu, Z. Ma, S.S. Mao, Ferromagnetism in GaN:Gd: a density functional theory study. Phys. Rev. Lett. **100**, 127203–127206 (2008)

20. S.K. Mandal, A.K. Das, T.K. Nath, D. Karmakar, Temperature dependence of solubility limits of transition metals (Co, Mn, Fe, and Ni) in ZnO nanoparticles. Appl. Phys. Lett. **89**, 144105 (2006)

21. B.B. Straumal, A.A. Mazilkin, S.G. Protasova, A.A. Myatiev, P.B. Straumal, B. Baretzky, Increase of Co solubility with decreasing grain size in ZnO. Acta Mater. **56**, 6246–6256 (2008)

22. W.M. Jadwisienczak, H.J. Lozykowski, A. Xu, B. Patel, Visible emission from ZnO doped with rare-earth ions. J. Electron. Mater. **31**, 776–784 (2002)

23. W. Jia, K. Monge, F. Fernandez, Energy transfer from the host to Eu3+ in ZnO. Opt. Mater. **23**, 27–32 (2003)

24. P.P. Murmu, R.J. Mendelsberg, J. Kennedy, D.A. Carder, B.J. Ruck, A. Markwitz, R.J. Reeves, P. Malar, T. Osipowicz, Structural and photoluminescence properties of Gd implanted ZnO single crystals. J. Appl. Phys. **110**, 033534–033539 (2011)

25. H. Wang, H.B. Wang, F.J. Yang, Y. Chen, C. Zhang, C.P. Yang, Q. Li, S.P. Wong, Structure and magnetic properties of Zn1-xCoxO single-crystalline nanorods synthesized by a wet chemical method. Nanotechnology **17**, 4312–4316 (2006)

26. T. Kataoka, Y. Yamazaki, Y. Sakamoto, A. Fujimori, F.H. Chang, H.J. Lin, D.J. Huang, C.T. Chen, A. Tanaka, S.K. Mandal, T.K. Nath, D. Karmakar, I. Dasgupta, Surface- and bulk-sensitive X-ray absorption study of the valence states of Mn and Co ions in Zn1−2×Mn×Co×O nanoparticles. Appl. Phys. Lett. **96**, 252502 (2010)

27. D. Karmakar, S.K. Mandal, R.M. Kadam, P.L. Paulose, A.K. Rajarajan, T.K. Nath, A.K. Das, I. Dasgupta, G.P. Das, Ferromagnetism in Fe doped ZnO: experiment and theory. Phys. Rev. B **75**, 144404 (2007)

28. B. Kumar, H. Gong, S. Vicknesh, S.J. Chua, S. Tripathy, Photoluminescence and multiphonon resonant Raman scattering in low-temperature grown ZnO nanostructures. Appl. Phys. Lett. **89**, 071922 (2006)

29. M.V. Limaye, S.B. Singh, R. Das, P. Poddar, S.K. Kulkarni, Room temperature ferromagnetism in undoped and Fe doped ZnO nanorods: microwave-assisted synthesis. J. Solid State Chem. **184**, 391–400 (2011)

30. A.K. Singh, V. Viswanath, V.C. Janu, Synthesis, effect of capping agents, structural, optical and photoluminescence properties of ZnO nanoparticles. J. Lumin. **129**, 874–878 (2009)

31. C.X. Xu, X.W. Sun, X.H. Zhang, L. Ke, S.J. Chua, Photoluminescent properties of copper-doped zinc oxide nanowires. Nanotechnology **15**, 856–861 (2004)

32. K. Vanheusden, C.H. Seager, W.L. Warren, D.R. Tallant, J.A. Voigt, Correlation between photoluminescence and oxygen vacancies in ZnO phosphors. Appl. Phys. Lett. **68**, 403–405 (1996)

33. J. Kennedy, P.P. Murmu, E. Manikandan, S.Y. Lee, Investigation of structural and photoluminescence properties of gas and metal ions doped zinc oxide single crystals. J. Alloy Comp. **616**, 614–617 (2014)

34. A.V. Dijken, E.A. Meulenkamp, D. Vanmaekelbergh, A. Meijerink, The kinetics of the radiative and nonradiative processes in nanocrystalline ZnO particles upon photoexcitation. J. Phys. Chem. B **104**, 1715–1723 (2000)

35. A.B. Djurišić, W.C.H. Choy, V.A.L. Roy, Y.H. Leung, C.Y. Kwong, K.W. Cheah, T.K. Gundu Rao, W.K. Chan, H.F. Lui, C. Surya, Photoluminescence and EPR of ZnO tetrapod structures. Adv. Funct. Mater. **14**, 856–864 (2004)

36. S.A. Studenikin, N. Golego, M. Cocivera, Fabrication of green and orange photoluminescent, undoped ZnO films using spray pyrolysis. J. Appl. Phys. **84**, 2287–2294 (1998)

37. R. Thangavel, R.S. Moirangthem, W.S. Lee, Y.C. Chang, P.K. Wei, J. Kumar, Cesium doped and undoped ZnO nanocrystalline thin films: a comparative study of structural and micro-Raman investigation of optical phonons. J. Raman Spectrosc. **41**, 1594–1600 (2010)

38. J. Wrzesinski, D. Frohlich, Two photon and three photon spectroscopy of ZnO under uniaxial stress. Phys. Rev. B **56**, 13087–13093 (1997)

39. P. Chetri, B. Saikia, A. Choudhary, Structural and optical properties of Cu doped SnO2 nanoparticles: an experimental and density functional study. J. Appl. Phys. 111, 233514/1–8 (2013)

40. S. Mehraj, M.S. Ansar, Alimuddin, Structural, electrical and magnetic properties of (Fe, Co) co-doped SnO$_2$ diluted magnetic semiconductor nanostructures. Phys. E **65**, 84–92 (2015)

41. J. Kennedy, G.V.M. Williams, P.P. Murmu, B.J. Ruck, Intrinsic magnetic order and inhomogeneous transport in Gd-implanted zinc oxide. Phys. Rev. B **88**, 214423–214427 (2013)

42. S. Kumar, P.D. Sahare, Gd3+ incorporated ZnO nanoparticles: a versatile material. Mater. Res. Bull. **51**, 217–223 (2014)

43. S. Venkatesh, J.B. Franklin, M.P. Ryan, J.S. Lee, H. Ohldag, M.A. McLachlan, N.M. Alford, I.S. Roqan, Defect-band mediated ferromagnetism in Gd-doped ZnO thin films. J. Appl. Phys. 117, 013913/1–6 (2015)

44. I. Bantounas, S. Goumri-Said, M.B. Kanoun, A. Manchon, I. Roqan, U. Schwingenschlögl, Ab initio investigation on the magnetic ordering in Gd doped ZnO. J. Appl. Phys. 109, 083929/1–7 (2011)

45. I. Bantounas, V. Singaravelu, I.S. Roqan, U. Schwingenschlogl, Structural and magnetic properties of Gd-doped ZnO. J. Mater. Chem. C **2**, 10331–10336 (2014)

46. P.P. Murmu, J. Kennedy, B.J. Ruck, G.V.M. Williams, A. Markwitz, S. Rubanov, A.A. Suvorova, Effect of annealing on the structural, electrical and magnetic properties of Gd-implanted ZnO thin films. J. Mater. Sci. **47**, 1119–1126 (2012)